Title
An Enskog based Monte Carlo method for high Knudsen number non-ideal gas flows

Journal
Computers & Fluids, 36(8)

ISSN
0045-7930

Authors
Wang, Moran
Li, Zhixin

Publication Date
2007-09-01

Peer reviewed

An Enskog based Monte Carlo method for high Knudsen number non-ideal gas flows

Moran Wang [†a,b], Zhixin Li [c]

[a] Department of Biological and Agricultural Engineering, University of California, Davis, CA 95616
[b] Department of Mechanical Engineering, The Johns Hopkins University, Baltimore, MD 21218
[c] Department of Engineering Mechanics, Tsinghua University, Beijing, 100084, China

Cited as: Moran Wang, Zhixin Li An Enskog based Monte Carlo method for high Knudsen number non-ideal gas flows *Computers & Fluids*, *Volume 36, Issue 8, September 2007*, *Pages 1291-1297*

[†] Corresponding author, Tel: 1-530-754-6770, Fax: 1-530-752-7584
Email: mmwang@ucdavis.edu

Abstract

A Monte Carlo method based on the Enskog equation for dense gas is developed by considering high density effect on collision rates and both repulsive and attractive molecular interactions for a Lennard-Jones fluid. The appropriate internal energy exchange model is introduced with consistency with the collision model. The equation of state for a non-ideal gas is therefore derived involving the finite density effect and the van der Waals intermolecular force, changing from the Clapeyron equation to the van der Waals equation. In contrast to previous Monte Carlo approaches, the present predictions agree better with experimental data for the gas transport properties at high densities and in a wide temperature region. The numerical modeling of non-ideal gas flow in micro- and nanochannels show that the high gas density affects greatly flow behavior and heat transfer characteristics. The high density of gas leads to a lower skin friction coefficient on the wall surfaces than the predictions by the perfect gas assumption.

Keywords: Monte Carlo method; gas flow; non-ideal gas flow; high Knudsen number; van der Waals equation

1. Introduction

When the mean free path of molecules is comparable to the characteristic length of a system in rarefied gas flows, the continuum assumption breaks down and the gas must be described by the Boltzmann equation [1]. The direct simulation Monte Carlo (DSMC) method is a particle-based numerical scheme for solving the nonlinear Boltzmann equation for the high Knudsen number gas flow [2-4]. It has been successfully applied for rarefied gas flows [4-7], and more recently for gas flows in micro- and nanoscale devices [8-15]. However, DSMC encounters the usual inconsistency of the Boltzmann equation; namely, it yields the transport properties for a rarefied hard sphere (HS) gas with a diameter σ, yet has an ideal gas equation of state (EOS) by implying σ=0 [16]. Alexander *et al*. [17] proposed a consistent Boltzmann algorithm (CBA), which modified DSMC by introducing an additional displacement in the advection process and an enhanced collision rate in order to obtain the van der Waals equation of state for dense gases [18]. The consistent Boltzmann algorithm has been used for simulation of nuclear flow [19], surface properties [20], and micro- and nanochannel flows [21,22]. However, it was found that the introduction of CBA into DSMC did not only revise the equation of state (EOS) but also changed the fluid transport properties [23].

As well known, Enskog presented the Enskog equation (EE) for hard spheres to incorporate finite-density effects [24]. He introduced two significant changes: the finite distance between the centers of a colliding pair; the increase of the collision frequency due to excluded volume effects. Based on EE, Montanero *et al*. [25-28] proposed an Enskog simulation Monte Carlo (ESMC) method which extended Bird's DSMC for a HS fluid at finite densities. However, in the ESMC methods, the attractive interactions between molecules were absent, and the transport properties from ESMC did not agree well with experimental data or the Enskog theoretical values.

In this work, an Enskog based Monte Carlo method is developed for simulations of the high Knudsen number non-ideal gas flows. After validation by comparing the predicted transport properties with experimental data and the Enskog theory, the Monte Carlo method is used to modeling the dense gas flow

in micro- and nanochannels. The physical mechanism in high density and high Knudsen number gas flows is therefore discussed.

2. Generalized Enskog Monte Carlo algorithm

In the present Monte Carlo method, a generalized collision model is introduced by considering the intermolecular Lennard-Jones potential and the denseness effects on the transport properties, so that the gas equation of state is extended from the Clapeyron equation to the van der Waals equation. The enhanced collision rate is determined by considering the excluded molecular volume and shadowing/screening effects based on the Enskog theory. The internal energy exchange model is also adapted to be consistent with the generalized collision model based on the Parker's formula.

2.1 Generalized collision model

In the standard DSMC method of Bird [2,3], the molecular interaction in variable hard sphere (VHS) or variable soft sphere (VSS) models was considered as only a repelling force. However in actual gases the force between two molecules is repulsive at small distances, and more weakly attractive at larger distances. This behavior is most simply described by the Lennard-Jones (6-12) potential [29]

$$\varphi(r) = 4\varepsilon\left[\left(\frac{\sigma}{r}\right)^{12} - \left(\frac{\sigma}{r}\right)^{6}\right], \tag{1}$$

where σ denotes the molecular diameter and ε is the depth of the potential well, which are constants characteristic of the chemical species of the colliding molecules; and *r* is the inter-molecular separation. This potential was proved adequate for a number of non-polar molecules. Many efforts have been paid to establish collision models to embody the Lennard-Jones potential in the molecular interaction process [30-33]. These models have defined the total collision cross section as

$$\frac{\sigma_T}{\sigma^2} = \sum \alpha_j \left(\frac{E_t}{\varepsilon}\right)^{-\omega_j}, \tag{2}$$

where σ_T is the total collision cross section, E_t denotes the relative translational energy, the

parameters ω_j are related to the Lennard-Jones potential [30-32], and α_j are determined from the transport property data, depending on whether the interaction is between like or unlike molecules.

The coefficients of viscosity, μ, and self-diffusion, D, of a simple gas to the first approximation, are expressed as functions of temperature by [29]

$$\mu = \frac{5}{16}\left(\frac{(\pi mkT)^{1/2}}{\pi\sigma^2\Omega^{(2,2)^*}}\right), \tag{3}$$

$$D = \frac{3}{16}\left(\frac{(2\pi kT/m_r)^{1/2}}{n\pi\sigma^2\Omega^{(1,1)^*}}\right), \tag{4}$$

where m is the particle mass, k the Boltzmann constant, n the number density, $m_r = m_1 m_2/(m_1+m_2)$ the reduced mass and $\Omega^{(1,1)^*}$ and $\Omega^{(2,2)^*}$ are integrals for calculating the transport coefficients for the Lennard-Jones potential [34]. For a L-J gas model with a total collision cross section given by Eq.(2), the self-diffusion and viscosity integrals are

$$\Omega^{(1,1)^*} = \frac{1}{\pi(\alpha^*+1)}\sum \alpha_j \Gamma(3-\omega_j) T_*^{-\omega_j}, \tag{5}$$

$$\Omega^{(2,2)^*} = \frac{\alpha^*}{\pi(\alpha^*+1)(\alpha^*+2)}\sum \alpha_j \Gamma(4-\omega_j) T_*^{-\omega_j}, \tag{6}$$

where α^* denotes the scattering coefficient for a soft-sphere model, $T_* = kT/\varepsilon$, and $\Gamma(...)$ denotes the gamma function. These definitions are related to the treatments given in Fan's GSS model [33] using the numerical solution for $\Omega^{(2,2)^*}$ tabulated in Table I-M of Hirschfelder *et al*. [34], with a two-term fit giving the five values of the parameters: α_1 = 3.962, α_2 = 4.558, ω_1 = 0.133, and ω_2 = 1.25 with $\alpha^* = 1.5$. These values are generally suitable for simple non-polar gas. For polar gases, the Stockmayer potential model can provide correct descriptions, which can be found in Ref [33] in detail.

In the standard Enskog theory, the pressure in a dense gas can be expressed as

$$p = knT\left[1+\eta\chi\right], \tag{7}$$

where $\eta = 2\pi n\sigma^3/3$ represents the gas molecular volume ratio, and χ is the collision enhancement factor dependent of the gas density.

However, Enskog preferred a different procedure based on the close relation between $(\eta \cdot \chi)$ and the compressibility. He observed that, if the molecules are surrounded by weak attractive force fields, the equation of state would be modified to the form following

$$p + a\rho^2 = knT\left[1 + \eta\chi\right], \tag{8}$$

where a denotes the strength of the attraction, which is dependent on the gas properties [24]

$$a = \frac{27}{64}\frac{R^2T_c^2}{p_c}, \tag{9}$$

where R denotes the gas constant, T_c the critical temperature, and p_c the critical pressure.

The transport properties of dense gases are therefore expressed in terms of the transport properties in ideal gases at ordinary densities and at a same temperature by the following relations [29]

$$\mu' = \mu \cdot \eta\left[(\eta\chi)^{-1} + 0.8 + 0.7614(\eta\chi)\right], \tag{10}$$

$$\kappa' = \kappa \cdot \eta\left[(\eta\chi)^{-1} + 1.2 + 0.7574(\eta\chi)\right], \tag{11}$$

where the prime values are the transport coefficients in a dense gas, and κ is the heat conduction coefficient.

2.2 Collision enhancement rate

The collision enhancement rate is an important parameter in dense gas theory and numerical simulations. Based on the Enskog equation for dense gases [24], when a gas is so dense that the *co*volume of the molecules is comparable with the total system volume, the molecules can no longer be treated as point particles. Therefore, the common position of two colliding molecules in the Boltzmann equation should be replaced by the actual positions of the centers of two tangent spheres. And the collision frequency is influenced by *c*orrelational effects that depend on the density at the point of contact.

Due to the reduced volume occupied by the molecules, a modified higher scattering probability, Π,

is

$$\Pi = (1 - 4n\pi\sigma^3 / 3)\Pi_B . \quad (12)$$

where Π_B is the scattering probability for rarefied gas based on the Boltzmann theory.

However, the scattering probability is lowered again by another effect that the particles are screening each other. A particle might not be available for scattering with another particle because there might be a third particle in between. This effect leads to a reduction of the scattering probability by a factor $\left(1 - 11n\pi\sigma^3 / 12\right)$. With this factor, the modified scattering probability is

$$\Pi = \chi \cdot \Pi_B , \quad (13)$$

where $\chi = \dfrac{1 - 11\eta/8}{1 - 2\eta}$.

This result can, however, be trusted only to the early orders of η, since four particle configurations have not been considered. The expression up to third order is [24]:

$$\chi(\eta) = 1 + 0.625\eta + 0.2869\eta^2 + 0.1103\eta^3 . \quad (14)$$

This expression's value is lower than those from the expression of Kortemeyer *et al.*[19], while close to that from Frezzotti *et al.* [27] and Garcia *et al.*[35-37] in the CBA introduction.

2.3 Internal energy exchange model

Since the flows considered involve internal energy, a model for internal energy exchange must be established. For the DSMC method, this is traditionally done with the Borgnakke-Larsen method [2,3]. Here the Borgnakke-Larsen model has to be modified for the generalized collision model.

The internal energy of a collision pair is the sum of the internal energies of the components

$$E_i = \varepsilon_{i,1} + \varepsilon_{i,2} . \quad (15)$$

The distribution function for the internal energy for a single molecule can be written as

$$f_{\varepsilon_{i,1}} \propto \varepsilon_{i,1}^{(\zeta_1/2)-1} \exp(\varepsilon_{i,1} / kT) , \quad (16)$$

where ζ_1 is the number of internal freedom degree of molecule 1. The total fraction of pairs with

internal energy E_i is proportional to f_E,

$$f_{E_i} \propto E_i^{\zeta-1} \exp(-E_i / kT), \tag{17}$$

where $\zeta = (\zeta_1 + \zeta_2)/2$. Based on a similar process, the distribution of the translational energy, E_t is given by

$$f_{E_t} = \frac{2}{m_r^2}\left(\frac{m_r}{kT}\right)^{3/2} \sqrt{(2/\pi)}\, \frac{\sigma_T}{\sigma_T c_r} E_t \exp(-E_t / kT). \tag{18}$$

The total energy E_c in the collision is combining the relative translational energy and the internal energy,

$$E_c = E_t + E_i .$$

The probability of a particular pair values E_t and E_i is proportional to the product of f_{E_t} and f_{E_i},

$$f_{E_t} f_{E_i} \propto \sigma_T E_t (E_c - E_t)^{\zeta-1} \exp(-E_c / kT). \tag{19}$$

For each inelastic collision, a post-collision value E_t^* is sampled from this distribution by the acceptance-rejection method. This needs finding the maximum of Eq. (19) and taking the ratio of Eq. (19) to its maximum. Let

$x = E_t / \varepsilon$, and $\xi = E_c / \varepsilon$,

then the maxima of Eq. (19) follow from determining the maximum of the quantity

$$G(x) = \left(\sum \alpha_j x^{1-\omega_j}\right)\left(\xi - x\right)^{\zeta-1}. \tag{20}$$

Setting the derivative of $G(x)$ to zero gives

$$(\xi - x)^{\zeta-2}\left\{\sum \alpha_j \left[(\omega_j - \zeta)x^{1-\omega_j} + \xi(1-\omega_j)x^{-\omega_j}\right]\right\} = 0. \tag{21}$$

Ignoring $x = \xi$, root x^* is found by iteration. The normalized distribution function is obtained from

$$F(x) = G(x) / G(x^*). \tag{22}$$

Regularly, this process needs numerical iteration which costs much in computing. Borrowing from the acceptance-rejection method in VHS model of the standard DSMC, one can implement this process by a Monte Carlo way. The random number, R_f (between 0 and 1), gives

$$E_t = R_f E_c, \quad E_i = E_c - E_t. \tag{23}$$

Substitute Eq. (23) into Eq. (22), and the value of F is compared with another R_f. If $F < R_f$, another R_f is made and the process is repeated. Otherwise, Eq. (23) is accepted.

The Borgnakke-Larsen model provides an average split of energies equal to the ratio of the DOF of the mode being partitioned to the total number of DOF to ensure detailed balance. Due to this, the f_{E_t} in Eq. (18) can be replaced by a Hinshelwood type distribution [3] with a ζ_t given from

$$E_t = (\zeta_t / 2)kT, \tag{24}$$

where $$\zeta_t = 2\left\{2 - \omega_1 + \frac{\omega_1 - \omega_2}{(\alpha_1/\alpha_2)\left[\Gamma(2-\omega_1)/\Gamma(2-\omega_2)\right](kT/\varepsilon)^{\omega_2-\omega_1}+1}\right\} \tag{25}$$

With this choice, all computational procedures employed in the VHS model of DSMC can be implemented for the generalized Monte Carlo method. The only additional complexity is that resulting from a calculation of a cell temperature. The simplification in the numerical procedure yields the correct macroscopic properties. However, the details of the distribution will be different because Eq. (18) is not exactly of the type indicated in Eq. (16).

Another crucial part of the Borgnakke-Larsen method is the determination of the inelastic collision probability. This probability used to be $P = 1/Z$, with Z representing the relaxation number; however, it is not true in general. The form of the probability function largely depends on the selection methodology used in employing the probability and the relaxation rate equation specified [30,31]. We use the probability formula for the pair selection methodology in the present model for rotational relaxation of Lumpkin's [38]:

$$P_r = (1 + \zeta_t / \zeta_r) / Z_R, \tag{26}$$

where ζ_t is the relative translational degree of freedom (DOF), ζ_r the sum of the rotational DOF of the colliding molecules, and Z_R the rotational relaxation number. The important notation of this formula is the pair selection methodology in which the probability is applied to the pair of colliding particles, and both relax if the event is accepted. This is in contract to the typical selection methodology used in Bird's particle selection method in which each colliding particle is checked for relaxation.

The temperature-dependent relaxation number for Z_R can be determined by the famous Parker's formula [39]. Hash *et al*. [31] gave the Parker's formula for a generalized hard sphere model as

$$Z_R = \frac{\left[\sum \alpha_j \left(\frac{T^*}{T}\right)^{\omega_j} \Gamma(2-\omega_j)\right] \frac{2-\omega_j}{2} Z_{R,\infty}}{\sum \alpha_j \left(\frac{T^*}{T}\right)^{\omega_j} \left[\frac{\Gamma(3-\omega_j)}{2} + \frac{2\pi}{3}\Gamma\left(\frac{5}{2}-\omega_j\right)\left(\frac{T^*}{T}\right)^{1/2} \Gamma(2-\omega_j)\left(\frac{T^*}{T}\right)\right]}. \qquad (27)$$

where $T^* = \varepsilon / k$, $Z_{R,\infty}$ is the limiting value of Z_R at high temperature, whose values for a few type of gas can be found in Ref. [40]. The expression reduces for the generalized hard sphere model to the original Parker's formula corrected by Brau and Jonkmann [41].

After the three steps, a generalized Enskog Monte Carlo (GEMC) model is thus established for the high Knudsen number non-ideal gas flows. The GEMC code is built up based on the standard DSMC code of Bird [3], and it can therefore share many developed techniques of DSMC such as indexing and sample techniques, and the no-time counter (NTC) method for collision pair selections.

3. Validations of the GEMC method

3.1 Transport coefficients

The GEMC method solves the Enskog equation for dense gas flows statistically with keeping the gas transport properties in good agreement with experimental data. The resulted transport coefficient viscosity is compared with values form previous methods and experimental data in Fig. 1 which shows the viscosity values versus temperatures for the nitrogen gas from different methods, together with the

experimental data which is from Table 16 and Table 28 in the reference [29]. The nitrogen molecular properties used here are: m=4.65×10^{-26} kg, σ =3.68×10^{-10} m, and ε / k =91.46 K [29]. The present method gives much better agreement with the experimental data at both low temperature and high temperature than other compared methods. Fig. 2 compares the viscosity values versus gas density between different models and experimental data for the nitrogen gas at 333 K under the pressure lower than 150 ×10^5 Pa. The viscosities from the GEMC model agree better with the experimental data than the ESMC results [3] and the CBA modifications with $d_{vdW} = \sigma$ [18,23] which deviate from the theoretical and experimental data greatly at high densities.

Therefore, the present method gives the best agreements with experimental data over a large range of temperature and densities.

[Insert Figure 1 here]

[Insert Figure 2 here]

3.2 GEMC vs. DSMC for low density gas flows

The current GEMC code was also validated by comparing the results with the standard DSMC code at low densities. Consider the nitrogen gas flowing in a short channel, shown in Fig. 3. The channel width is 0.01 μm. The aspect ratio L/H is 5.0 with uniform rectangular cells (100×60) used. The coming freestream gas has a temperature T_∞ =300 K and a velocity u_∞ =200 m/s. The number density of coming gas is n_∞ =5 n_0 with n_0 representing the number density of gas at the standard pressure and temperature, which leads to η_∞ =0.0135 and Kn_∞ =1.28. The details of DSMC implement and parameters can be found in Ref. [42,43]. In GEMC, the molecular parameters were: $\sigma = 3.681\times10^{-10}$ m, and $\varepsilon / k = 91.5$ K [33,34]; the critical temperature and pressure were: $T_c = 126.1$K, and p_c =3.39×10^6 Pa respectively [44]; the parameters in energy exchange model were: $Z_{R,\infty} = 18$ with $\varepsilon / k = 91.5$K [30,31,40] for the nitrogen gas. The subcell size is always smaller than the local gas mean free path and the time step is smaller than the local mean collision time to ensure the accuracies of simulations [43].

Both DSMC and GEMC calculations involved over 1×10^5 molecules in the domain and over 5×10^5 samples for stead smooth solutions. We compare the velocity and temperature profiles at inlet and outlet between the GEMC and DSMC methods in Fig. 4. The results show that the GEMC agree pretty well with the DSMC when the density effect is small enough to be ignored. This validates the correctness of the GEMC code.

[Insert Figure 3 here]

[Insert Figure 4 here]

4. Non-ideal gas flow in micro- and nanochannels

As the rapid developments of M/NEMS techniques, gas flows in micro- and nanochannels are often encountered in practice. The big flow resistance caused by the huge aspect ratio of micro- and nanochannels usually requests a big driving pressure, which actually make the gas dense. However the small characteristic length of the channel lead to a high Knudsen number that breaks the continuum-based theories and prediction methods down. Such flows with both high Knudsen numbers and high densities have never been effectively and correctly predicted though many efforts have been made in the past decade [18-22,25-27,49]. Here we present our results of such flow using the GEMC method.

[Insert Figure 5 here]

Again, let us consider the nitrogen gas subsonic flows in microchannels as shown in Fig. 3. A freesteam gas flows passing through the channel. The flow has certain density, temperature and velocity away from the channel. We increase the number density of coming gas up to $100\,n_0$, which leads to η_∞=0.135 and Kn_∞=0.06. Fig. 5 compares the simulation results of velocity and temperature profiles at inlet and outlet. The ESMC, DSMC and CBA results are also plotted in the same figures. The results show that the high gas density affects the flow and heat transfer characteristics deviating from predicted by the perfect gas assumption.

We noticed that the ESMC algorithm modified a lot on the enhanced particle collision but little on the internal energy exchange. Therefore its results agree well with the GEMC results in velocity profiles at inlet and outlet but deviate remarkable from the GEMC in the temperature field. At the same time, the reversal temperature distributions near the wall surface do not occur in the GEMC results as they do in the CBA simulations [21,22], which indicate that additional collision process should be modified to deal with the interaction between molecules and wall surfaces after the additional displacement in CBA. As a result, the present GEMC works better than the other two popular numerical methods for modeling of high Knudsen number non-ideal gas flows.

[Insert Figure 6 here]

Fig. 6 compares the skin friction coefficient distributions along the wall surfaces predicted by GEMC and DSMC methods. The results show that the density effect reduces the friction below the predictions of the perfect gas assumption. This result need experimental validations and the mechanism will be discussed in the future.

5. Conclusions

A generalized Enskog Monte Carlo method has been developed by introducing a generalized molecular collision model for Lennard-Jones potential and the corresponding internal energy exchange model into the Monte Carlo method for the correct modeling and predictions of high Knudsen number non-ideal gas flow and heat transfer. The generalized collision model considers both repulsive and attractive forces between molecules and the density effect, so that the gas equation of state extends from the Clapeyron equation to the van der Waals equation. The GEMC method was validated by comparing the gas transport properties with existing experimental data and by comparing numerical results with DSMC at low gas densities. The GEMC method was then used for simulations and analyses of non-ideal gas flows in micro- and nanochannels. The results show that the high gas density influences the flow

behavior and heat transfer deviating from the predictions by the DSMC method. The denseness makes the surface friction coefficient on the wall lower than that based on the perfect assumption.

Acknowledgements

The present work was supported by the National Natural Science Foundation of China (Grant No. 59995550-2).

References

[1] Gad-el-Hak M. The Fluid Mechanics of Microdevices—The Freeman Scholar Lecture. J Fluid Engin 1999; **121**: 5-33.

[2] Bird GA. Molecular gas dynamics. Oxford: Clarendon Press; 1976.

[3] Bird GA. Molecular Gas Dynamics and the Direct Simulation of Gas Flows. Oxford: Clarendon Press; 1994.

[4] Shen C. Raredied Gas Dynamics. Beijing: National Defense Industry Publishing House; 2003.

[5] Wagner W. A convergence proof for Bird's direct simulation Monte Carlo method for the Boltzmann equation. J Stat Phys 1992; **66**: 1011-1044.

[6] Bird GA. Recent advances and current challenges for DSMC. Comput Math Appl 1998; **35:** 1-14.

[7] Oran ES, Oh CK, Cybyk BZ. Direct Simulation Monte Carlo: Recent Advances and Applications. Annu Rev Fluid Mech 1998; **30**: 403-441.

[8] Karniadakis GE, Beskok A, Aluru NR. Microflows and Nanoflows: Fundamentals and Simulation. New York: Springer; 2005.

[9] Oh CK, Oran ES, Sinkovits RS. Computations of High-Speed, High Knudsen Number Microchannel Flows. J Thermophys. Heat Transfer 1997; **11**: 497-505.

[10] Liou WW, Fang Y. Heat Transfer in Microchannel Devices Using DSMC. J MicroElectroMech Syst. 2001; **10**: 274-279.

[11] Hadjiconstantinou NG, Simek O. Constant-Wall-Temperature Nusselt Number in Micro and Nano-Channels. J Heat Transfer. 2002; **124**: 356-364.

[12] Cai CP, Boyd ID, Fan J. Direct simulation methods for low-speed microchannel flows. J Thermophys Heat Transfer. 2000; **14**: 368-378.

[13] Fan J, Shen C. Statistical simulation of low-speed rarefied gas flows. J Comput Phys. 2001; **167**: 393-412.

[14] Wang X, Wang QW, Tao WQ, Zheng P. Simulation of rarefied gas flow and heat transfer in microchannels. Sci. in China Ser E 2002; **45**(3): 321-327.

[15] Wang M, Li ZX. Gas Simulations for Gas Flows in Microgeometries Using the Direct Simulation Monte Carlo Method. Int J Heat Fluid Flow 2004; **25**(6): 975-985.

[16] Baras F, Mansour MM, Garcia AL. Microscopic Simulation of Dilute Gases with Adjustable Transport-Coefficients. Phys Rev E 1994; **49:** 3512-3515.

[17] Alexander FJ, Garcia AL, Alder BJ. A Consistent Boltzmann Algorithm. Phys Rev Lett 1995; **74:** 5212-5215.

[18] Garcia AL, Wagner W. Some new properties of the kinetic equation for the consistent Boltzmann algorithm. Transport Theo Stat 2002; **31**: 579-594.

[19] Kortemeyer G, Daffin F, Bauer W. Nuclear flow in consistent Boltzmann algorithm models. Phys Lett B 1996; **374**: 25-30.

[20] Alexander FJ, Garcia AL, Alder BJ. The consistent Boltzmann algorithm for the van der Waals equation of state. Physica A 1997; **240**: 196-201.

[21] Wang M, Li ZX. Non-ideal gas flow and heat transfer in micro and nano channels using the direct simulation Monte Carlo method. Phys. Rev. E. 2003; **68**: 046704.

[22] Wang M, Li ZX. Micro and Nano Dense Gas Poiseuille Flow in a Consistent Boltzmann Algorithm Model. J Micromech Microengin 2004; **14**(7): 1057-1063.

[23] Garcia AL, Alexander FJ, Alder BJ. A particle method with adjustable transport properties-the generalized consistent Boltzmann algorithm. J Stat Phys 1997; **89**: 403-409.

[24] Schram PPJM. Kinetic Theory of Gas and Plasmas. Dordrecht: Kluwer Academic Pulishers; 1991.

[25] Montanero JM, Santos A. Monte Carlo simulation method for the Enskog equation. Phys Rev E 1996; **54**: 438-444.

[26] Montanero JM, Santos A. Simulation of Enskog Equation a la Bird. Phys Fluids 1997; **9**(7): 2057-2060.

[27] Frezzotti A. Particle scheme for the numerical solution of the Enskog equation. Phys Fluids 1997; **9**(5):1329-1335.

[28] Carnahan NF, Starling KE. Equation of State for Nonattracting Rigid Spheres. J Chem Phys 1969; **51**: 635.

[29] Chapman S, Cowling TG. The Mathematical Theory of Non-uniform Gases-Third Edition. Cambridge: Cambridge Universiyt Press; 1970.

[30] Hassan HA, Hash DB. A Generalized Hard-Sphere Model for Monte Carlo Simulation. Phys Fluids A 1993; **5**: 738-744.

[31] Hash DB, Moss JN, Hassan HA. Direct Simulation of Diatomic Gases using the Generalized Hard-Sphere Model. J Thermophys Heat Transfer. 1994; **8**: 758-764.

[32] Macrossan MN, Lilley CR. Modified generalized hard sphere collision model for direct simulation Monte Carlo calculations. J Thermophys Heat Transfer. 2003; **17**: 289-291.

[33] Fan J. A generalized soft-sphere model for Monte Carlo simulation. Phys Fluids 2002; **14**(12): 4399-4405.

[34] Hirschfelder JO, Curtiss CF, Bird RB. Molecular Theory of Gases and Liquids. Wiley: New York; 1954.

[35] Garcia AL, Baras F. Direct simulation Monte Carlo: Novel application and new extensions. In: Proceedings of the 3rd Workshop on Modelling of Chemical Reaction Systems, Heidelberg; 1997.

[36] Erpenbeck JJ, Wood WW. Molecular-Dynamics Calculations of the Hard-Sphere Equation of State. J Stat Phys 1984; **35**: 321-340.

[37] Erpenbeck JJ, Wood WW. Molecular-Dynamics Calculations of the Velocity Auto-correlation Function – Hard-sphere results. Phys. Rev. A, 1985, 32 (1): 412-422.

[38] Lumpkin FE, Haas BL, Boyd ID. Resolution of Differences between Collision Number in Particle and Continuum Simulations. Phys Fluids 1991; **3:** 2282-2284.

[39] Parker JG. Rotational and Vibrational Relaxation in Diatomic Gases. Phys Fluids. 1959; **2**: 449.

[40] Monchick L, Mason EA. Transport Properties of Polar Gases. J Chem. Phys. 1961; **35**: 1676.

[41] Brau CA, Jonkman RM. Classical Theory of Rotational Relaxation in Diatomic Gases. J Chem Phys. 1970; **52:** 477.

[42] Wang M, Li ZX. Similarity of ideal gas flow at different scales. Science in China Ser E 2003; **46**(6): 661-670.

[43] Wang MR, Li ZX. Gas Mixing in Microchannels using the direct simulation Monte Carlo method. Int. J. Heat Mass Transfer. 2006; **49**(9-10): 1696-1702.

[44] Aston JG., Fritz JJ. Thermodynamics and Statistical Thermodynamics. New York: John Wiley & Sons; 1959.

[45] Gatzen HH. Rigid disk slider micromachining challenges to meet microtribology needs. Tribol Int. 2000; **33:** 337-342.

[46] Zhang B, Nakajima A. Possibility of surface force effect in slider air bearings of 100 Gbit/in(2) hard disks Tribol Int. 2003; **36:** 291-296.

[47] Li XH, Du HJ, Liu B, Lau GK. Numerical simulation of slider air bearings based on a mesh-free method for HDD applications. Microsystem Technologies. 2005; **11:** 797- 804.

[48] Wang MR, Li ZX. Numerical simulations on performance of MEMS-based nozzles at moderate or low temperatures. Microfluidics and Nanofluidics, 2004; **1** (1): 62-70.

[49] Wang M, Li ZX. Monte Carlo simulations of dense gas flow and heat transfer in micro- and nano-channels. Science in China Ser E-Engineering & Materials Science 2005; **48**(3): 317-325.

Figure Captions

FIG. 1 Viscosity variations with temperature at low or moderate gas densities.

FIG. 2 Viscosity variations with density for the nitrogen gas at 333 K below 150×10^5 Pa.

FIG. 3 Schematic of the physical problem: H =0.01 μm, L/H =5.0, T_∞ =300 K, u_∞ =200 m/s, T_w =300 K with completely diffusion reflection at both wall surfaces.

FIG. 4 Comparison between the GEMC and DSMC results for a low density at η_∞ =0.0135 and Kn_∞ =1.28.

FIG. 5 Density effects on gas flow and heat transfer by GEMC, compared with DSMC, CBA, and ESMC results.

FIG. 6 Skin friction coefficient distributions along the wall surfaces as predicted by the GEMC and DSMC methods at η_∞ =0.135 and Kn_∞ =0.06.

Figure 1, Wang and Li, Computer & Fluids

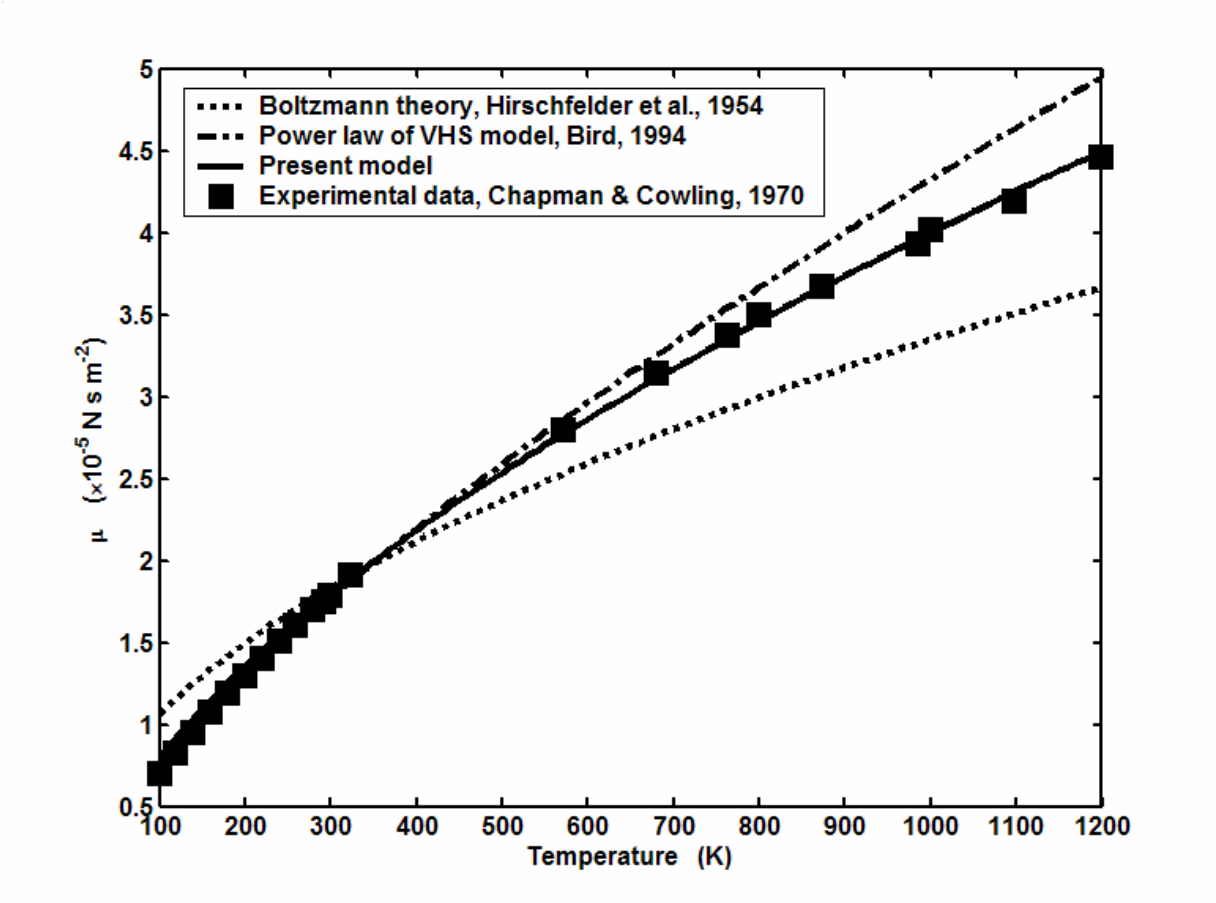

Viscosity variations with temperature at low or moderate gas densities

Figure 2, Wang and Li, Computer & Fluids

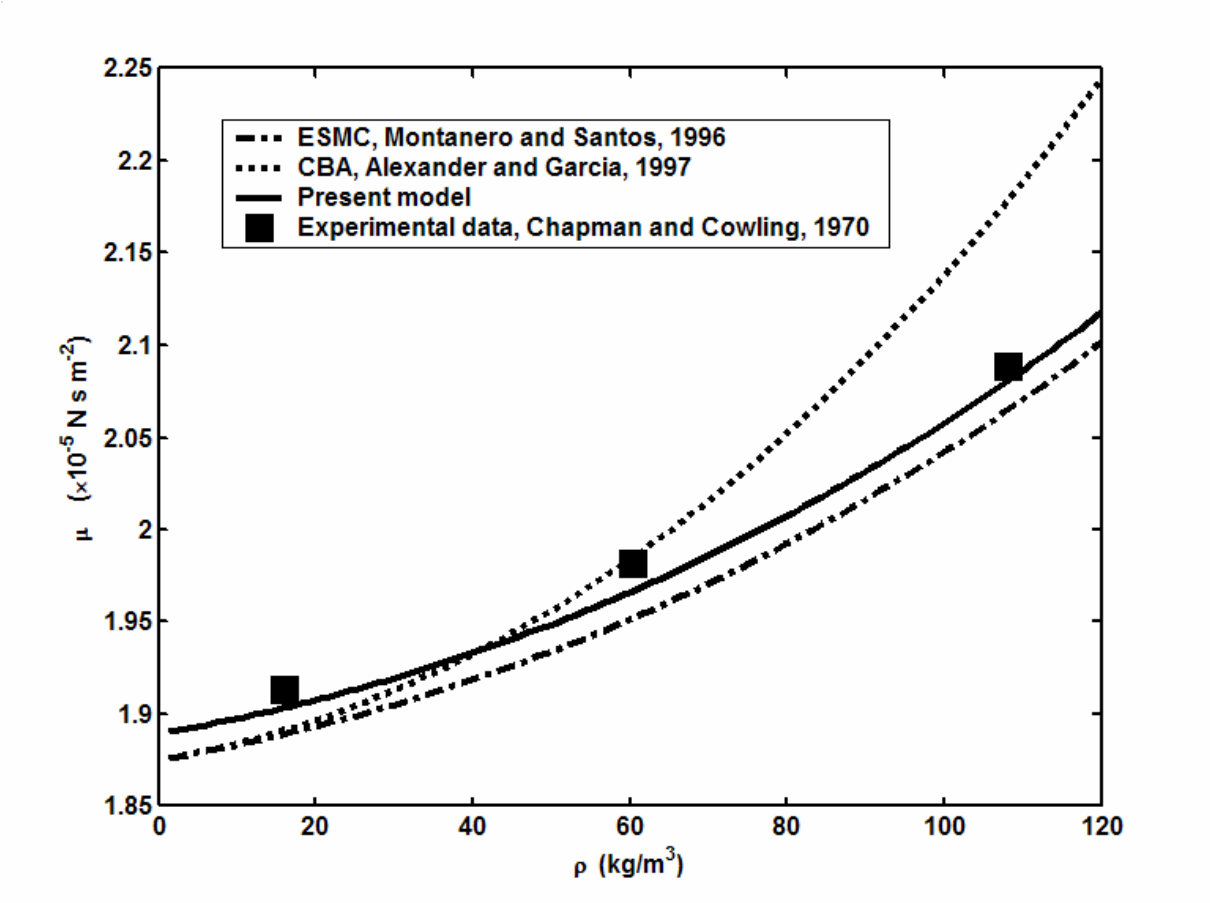

Viscosity variations with density below 150 $\times 10^5$ Pa at 333 K.

Figure 3, Wang and Li, Computer & Fluids

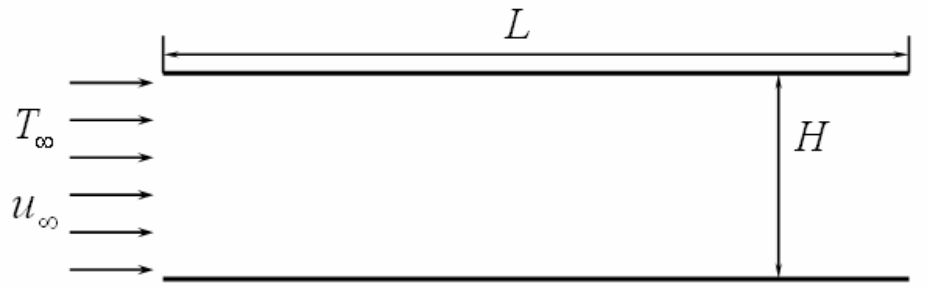

Schematic of the physical problem: H =0.01 μm, L/H =5.0, T_∞ =300 K, u_∞ =200 m/s, T_w =300 K with completely diffusion reflection at both wall surfaces.

Figure 4, Wang and Li, Computer & Fluids

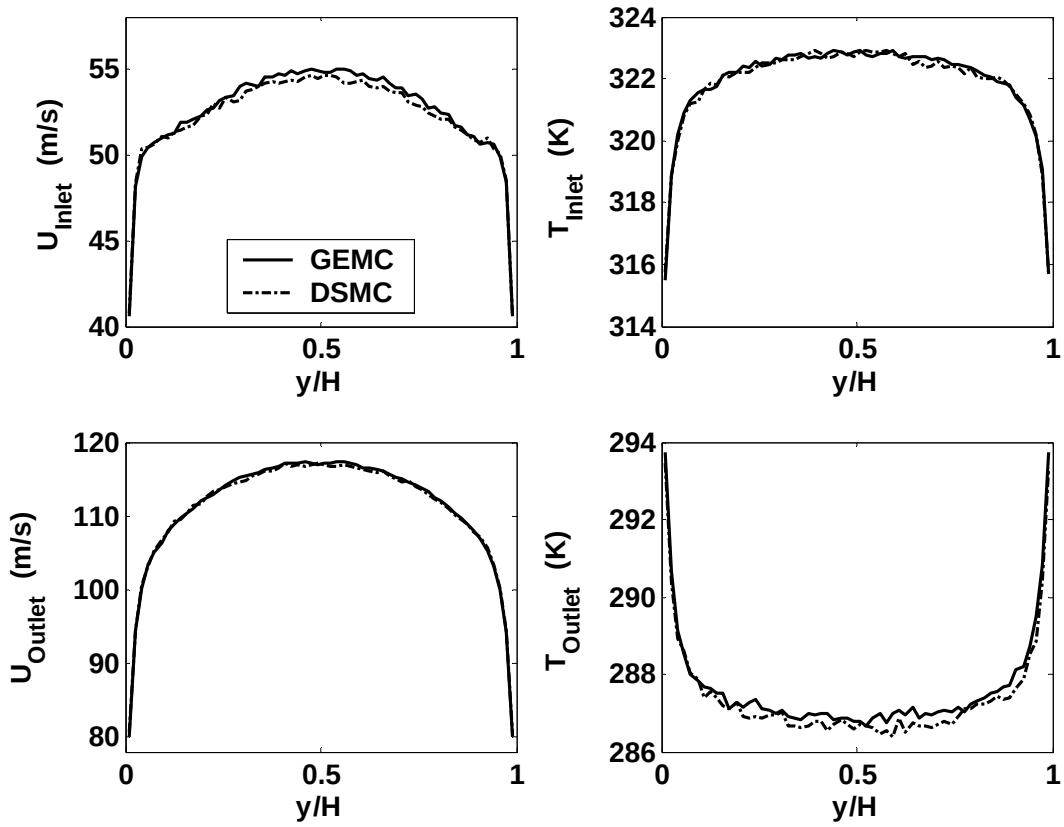

Comparisons between the GEMC and DSMC results for a low gas density at η_∞ =0.0135 and Kn_∞ =1.28.

Figure 5, Wang and Li, Computer & Fluids

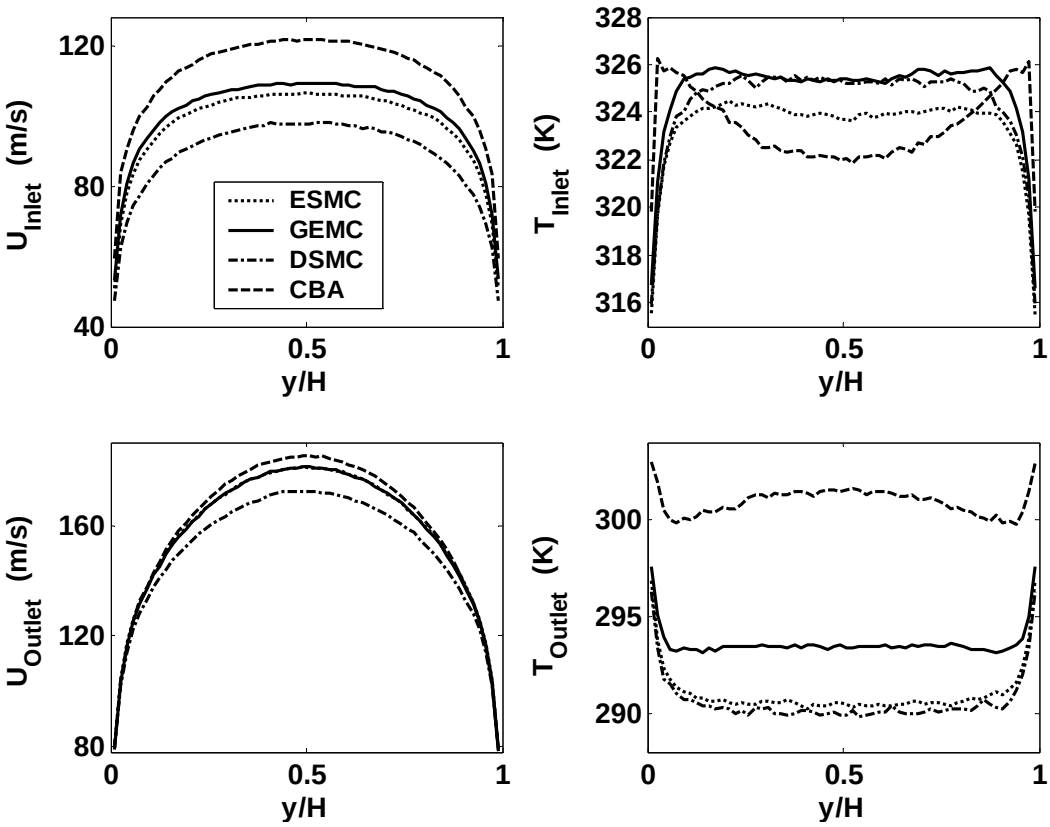

Density effects on gas flow and heat transfer by the GEMC method at η_∞ =0.135 and Kn_∞ =0.06, compared with DSMC, CBA, and ESMC results.

Figure 6, Wang and Li, Computer & Fluids

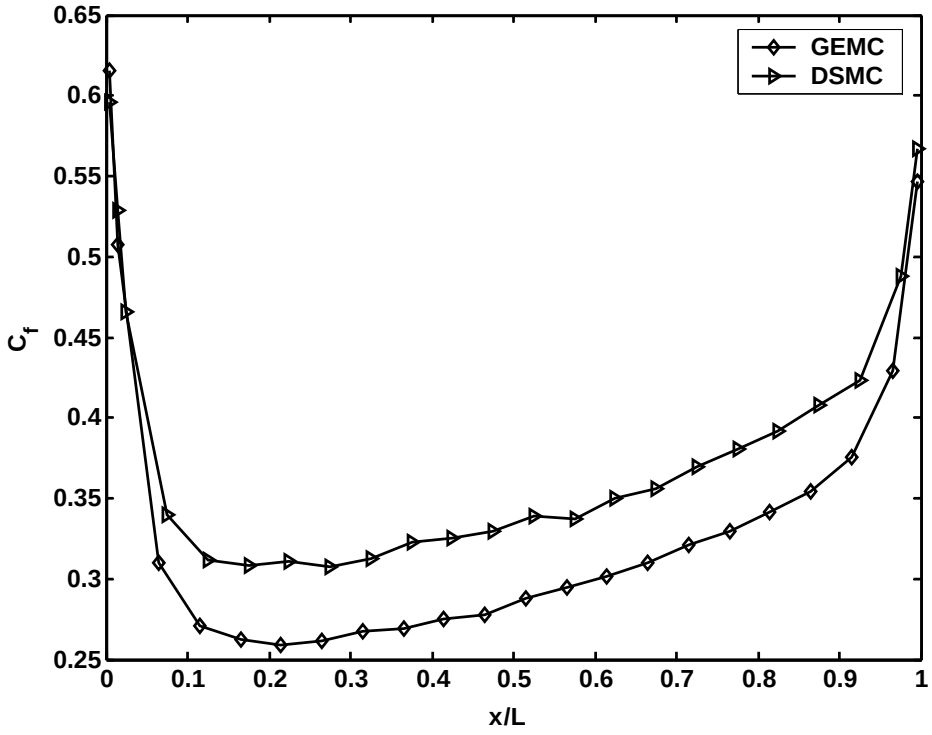

Skin friction coefficient distributions along the wall surfaces as predicted by the GEMC and DSMC methods at η_∞ =0.135 and Kn_∞ =0.06